Characteristics of precipitating energetic ions/electrons associated with the wave-particle interaction in the plasmaspheric plume

Zhigang Yuan,[1,2] Ying Xiong,[1] Dedong Wang,[1] Ming Li,[1] Xiaohua Deng,[1,3] A. G. Yahnin,[4] T. Raita,[5] and Jingfang Wang[1]

Received 30 March 2012; revised 12 June 2012; accepted 9 July 2012; published 22 August 2012.

[1] In this paper, we present characteristics of precipitating energetic ions/electrons associated with the wave-particle interaction in the plasmaspheric plume during the geomagnetic storm on July 18, 2005 with observations of the NOAA15 NOAA16, IMAGE satellites and Finnish network of search coil magnetometers. Conjugate observations of the NOAA15 satellite and the Finnish network of search coil magnetometers have demonstrated that a sharp enhancement of the precipitating ion flux is a result of ring current (RC) ions scattered into the loss cone by EMIC waves. Those precipitating RC ions lead to a detached subauroral proton arc observed by the IMAGE FUV. In addition, with observations of NOAA15 and NOAA16, the peak of precipitating electron flux was equatorward to that of precipitating proton flux, which is in agreement with the region separation of ELF hiss and EMIC waves observed by the Cluster C1 in the Yuan et al. (2012) companion paper. In combination with the result of the companion paper, we demonstrate the link between the wave activities (ELF hiss, EMIC waves) in plasmaspheric plumes and energetic ion/electron precipitation at ionospheric altitudes. Therefore, it is an important characteristic of the plasmaspheric plumes-RC-ionosphere interaction during a geomagnetic storm that the precipitation of energetic protons is latitudinally separated from that of energetic electrons.

Citation: Yuan, Z., Y. Xiong, D. Wang, M. Li, X. Deng, A. G. Yahnin, T. Raita, and J. Wang (2012), Characteristics of precipitating energetic ions/electrons associated with the wave-particle interaction in the plasmaspheric plume, *J. Geophys. Res.*, *117*, A08324, doi:10.1029/2012JA017783.

1. Introduction

[2] It is well known that a plasmaspheric drainage plume can be formed and extend from the main plasmasphere in the dusk sector to dayside magnetopause during geomagnetic storms [*Elphic et al.*, 1997; *Darrouzet et al.*, 2009]. The shape and location in magnetic local time of a given plume can be described in terms of phases that follow the rise and fall of convection strength [*Goldstein and Sandel*, 2005].

[3] Electromagnetic ion cyclotron (EMIC) waves are generated by a resonant interaction with ring current (RC) ions [e.g., *Cornwall*, 1965; *Horne and Thorne*, 1993; *Fraser and Nguyen*, 2001; *Gamayunov and Khazanov*, 2008]. The major source of free energy driving this instability is considered to be provided by energetic and anisotropic ring current protons [*Anderson et al.*, 1992; *Erlandson and Ukhorskiy*, 2001; *Sakaguchi et al.*, 2008]. The anisotropic proton distributions can become unstable to the amplification of EMIC waves. In presence of cold dense ions, the instability threshold is so low that EMIC waves are easily generated [*Gary et al.*, 1995]. Not only the plasmapause but also plasmaspheric plumes with steep density gradients are the preferred sites for the generation of EMIC waves [*Anderson et al.*, 1992; *Fraser and Nguyen*, 2001; *Morley et al.*, 2009]. Observations of the CRRES spacecraft have shown that occurrence of EMIC waves predominates in the afternoon sector [*Fraser and Nguyen*, 2001]. As a consequence of the EMIC waves-RC interaction, ring current protons can be scattered into the loss cone and cause subauroral arcs [*Jordanova et al.*, 2007; *Yahnin et al.*, 2009; *Spasojević and Fuselier*, 2009]. The tendency for subauroral arcs is demonstrated to be located in the mid-afternoon sector during disturbed periods, where plasmaspheric plumes can extend sunward from the main plasmasphere [*Immel et al.*, 2002; *Burch et al.*, 2002; *Spasojević et al.*, 2004; *Yuan et al.*, 2010].

[4] As a broadband, structureless, extremely low frequency (ELF) electromagnetic emission with whistler mode, plasmaspheric hiss have been observed in higher density regions associated with the Earth's plasmasphere [*Russell et al.*, 1969; *Thorne et al.*, 1973; *Cornilleau-Wehrlin et al.*, 1993;

[1]School of Electronic Information, Wuhan University, Wuhan, China.
[2]State Key Laboratory of Space Weather, Chinese Academy of Sciences, Beijing, China.
[3]Institute of Space Science and Technology, Nanchang University, China.
[4]Polar Geophysical Institute, Kola Science Centre, Russian Academy of Sciences, Apatity, Russia.
[5]Sodankylä Geophysical Observatory, University of Oulu, Oulu, Finland.

Corresponding author: Z. Yuan, School of Electronic Information, Wuhan University, Wuhan, 430072, China. (y_zgang@vip.163.com)

0148-0227/12/2012JA017783

Bortnik *et al.*, 2008] or detached plasma regions [*Chan and Holzer*, 1976; *Cornilleau-Wehrlin et al.*, 1978; *Parrot and Lefeuvre*, 1986]. One of the consequences of the ELF hiss-RC interaction is the precipitation of energetic electrons into the atmosphere due to pitch angle diffusion [*Titova et al.*, 1998; *Summers et al.*, 2008; *Yuan et al.*, 2011]. Energetic ion/electron precipitations associated with plasmaspheric plumes have been observed by the NOAA satellites at ionospheric altitudes [*Yahnin et al.*, 2006; *Yahnin and Yahnina*, 2007]. To our knowledge, few conjugate observations have been shown that both ELF hiss and EMIC waves in plasmaspheric plumes and energetic ion/electron precipitation observed by low-altitude satellites at ionospheric altitudes, which is very important to reveal the coupling process in the system of RC-plasmasphere-ionosphere through the wave-particle interactions.

[5] In the previous paper [*Yuan et al.*, 2012], we present wave and particle observations made by Cluster C1 satellite in a plasmaspheric plume in the recovery phase of the geomagnetic storm on July 18, 2005. Cluster C1 simultaneously observed EMIC waves and ELF hiss in the plasmaspheric plume. In the outer boundary of the plasmaspheric plume, Cluster C1 observed RC ions scattered into the loss cone by EMIC waves. The ELF hiss and EMIC waves are spatially separated: the ELF hiss is located in the vicinity of the electron density peak within the plume while the EMIC waves are detected in the outer boundary of the plume. This separation is likely a consequence of different characteristics of the electron and ion cyclotron wave-particle interaction and wave propagation (see, for example, results of modeling by *Pasmanik et al.* [1998], *Morley et al.* [2009], and *Chen et al.* [2010]). Since ELF hiss and EMIC waves are spatially separated, it is expected that the precipitation of energetic protons is latitudinally separated from that of energetic electrons due to wave-particle interaction. In order to better demonstrate the relationship between the wave activities (ELF hiss, EMIC waves) and energetic ion/electron precipitation in plasmaspheric plumes, conjugate observations of the Cluster satellite in the plasmasphere and low-altitude satellites (such as NOAA POES) at ionospheric altitudes are necessary. In this paper, we refer to our previous paper [*Yuan et al.*, 2012] as paper 1. We show the conjugate observations of the NOAA and IMAGE satellites associated with observations of Cluster C1 in paper 1.

[6] In this paper, we focus on characteristics of precipitating energetic ions/electrons associated with the wave-particle interaction in the plasmaspheric plume during the geomagnetic storm on July 18, 2005. In section 2, we briefly describe the instrumentation, including the NOAA SEM-2, IMAGE FUV instrument and Finnish network of search coil magnetometers. In section 3, we present observations of the NOAA 16 NOAA 15 and three selected stations of Finnish network on July 18, 2005. In section 4, these results are discussed and a summary is given.

2. Instrumentation

[7] The NOAA spacecraft have a polar orbit at ~800–850 km altitude. Each orbit takes about 103 min. Beginning with the NOAA 15 satellite, an upgraded version of the Space Environment Monitor (SEM-2) is being flown. The SEM-2 instrument package onboard the NOAA spacecraft, includes the Medium Energy Proton and Electron Detector (MEPED) and the Total Energy Detector (TED). Since the MEPED instrument has two detectors oriented approximately one along and another perpendicularly to the magnetic field at high geomagnetic latitudes (>50°), it can measure both trapped (at the satellite's altitude) and precipitating particles [*Sandanger et al.*, 2007]. The MEPED instrument measures the energetic electron in three channels (>30 keV (e1), >100 keV (e2), and >300 keV (e3)) and energetic proton in six channels (30–80 keV (P1), 80–240 keV (P2), 240–800 keV (P3), 800–2500 keV (P4), 2500–6900 keV (P5), >6900 keV (P6)). *Raben et al.* [1995] describe the spacecraft and instrumentation. All NOAA data are available from http://NOAA.ngdc.noaa.gov/data/. The full resolution data has 2 s time resolution, which we use in this paper.

[8] The ground observations of geomagnetic pulsations at the Kilpisjarvi (KIL) Ivalo (IVA) and Sodankylä (SOD) observatories were performed by the Finnish network of search coil magnetometers located at MLT = UT + 2. Data sampling frequency is 40 Hz. The magnetometers of the Finnish chain have over the same frequency range a linear frequency response of 1.4 V/(nT*Hz) with an instrumental noise figure of ~1 $pT/Hz^{1/2}$ at 1 Hz. The magnetometers of the Finnish network are identical and can be used for comparison of intensity of the pulsation at those three stations.

[9] Since the SI12 channel of the IMAGE FUV instrument was designed to select the Doppler shifted Lyman H-alpha line at 121.82 nm and to reject the non-Doppler shifted Lyman H-alpha from the geocorona at 121.567 nm [*Mende et al.*, 2000], the observed emissions mainly come from charge-exchanging precipitating protons.

3. Observations

[10] Locations of the selected Finnish network of search coil magnetometers and the magnetic footprints of Cluster C1 and NOAA 15 NOAA 16 mapped to the ground (Cluster 1 between 14:45 and 15:00 UT, NOAA 15 between 14:51 and 14:55 UT, NOAA 16 between 14:45 and 14:57 UT) are shown in Figure 1. Figure 1 shows that the footprint of the NOAA 15 and three stations with search coil magnetometers almost belong to the same meridional plane during the interval, which enables the conjugate observations of the NOAA15 satellite and three ground-based stations. On the other hand, the footprint of Cluster C1 in longitudes (in MLT of Table 1) is located between that of NOAA 15 and that of NOAA 16.

[11] It is necessary to compare intensities of precipitating fluxes with those of trapped fluxes in order to characterize the anisotropy of the particle pitch angle distribution [*Titova et al.*, 1998]. In Figure 2, blue and red lines show the trapped and precipitating flux intensities observed by the MEPED instrument of the NOAA 15, respectively. The black vertical solid line denotes the poleward boundary of the proton anisotropic zone, which is also the equatorial boundary of the proton isotropic zone at higher (auroral) latitudes. The energetic proton flux isotropization in the proton isotropic zone at higher latitudes is due to the particle scattering into the loss cone in the magnetospheric equatorial plane where the magnetic field is weak and the particle gyroradius is comparable with the field line curvature radius [*Sergeev et al.*, 1983]. Within the anisotropic zone, a sharp enhancement of the

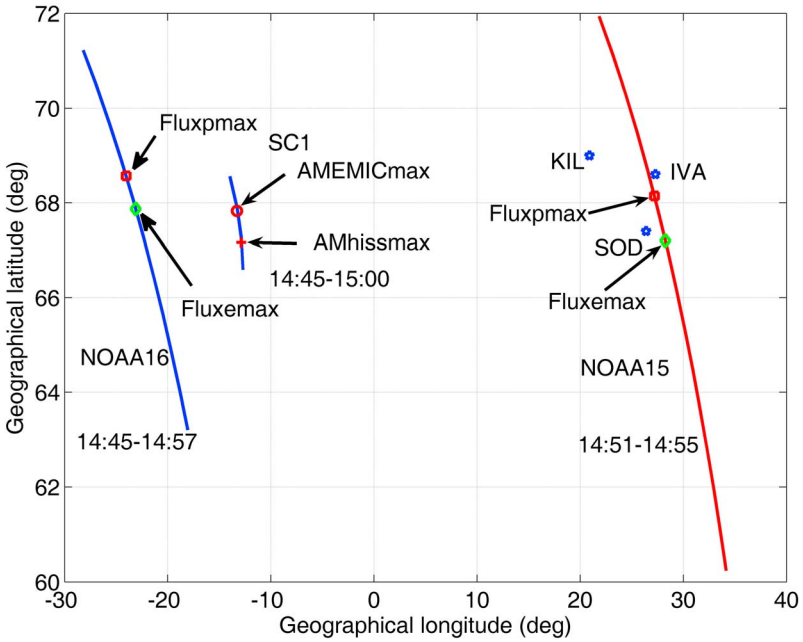

Figure 1. Locations of three stations (KIL IVA SOD MLT = UT + 2) with search coil magnetometers and footprints of the Cluster C1, NOAA 15 and NOAA 16 mapped to the ground. Blue stars indicate three sites with search coil magnetometers. The blue square and green diamond denote the location of peak flux for precipitating protons and electrons observed by the NOAA 15 and NOAA 16, respectively. The red circle and plus denote the location of peak amplitude for EMIC and ELF hiss waves observed by the Cluster C1, respectively.

precipitating ion flux, together with the prominent variation of the trapped flux intensity, is seen at 14:53:45 UT. As denoted by the yellow vertical solid line in Figure 2, the peak of precipitating proton flux was located at 68.15° geographical latitude (64.43° geomagnetic latitude). In this case, we can see that the precipitating flux in the first channel (Figure 2, first panel) is almost as intense as the mirroring flux, which serves as an indication of strong pitch angle scattering for ions with energies between 30 keV and 80 keV, while for the higher energies pitch angle diffusion is weaker.

[12] As noted *Evans and Greer* [2004], the SEM-2 e1, e2, and e3 telescopes suffer from contamination by rather low energy protons, with one proton in the correct energy range leading to one count in the electron detector. In order to quantify the level of contamination in the e1, e2, and e3 telescopes, and estimate where the counts from the "electron" telescopes are most likely to be dominated by electrons, the condition is required that the counts reported by the electron telescope be at least twice as large as the counts from the "contaminating" proton telescope because one "contaminating" proton will produce one incorrect electron count [*Rodger et al.*, 2010].

[13] Under these conditions, the electron observations are taken to be "good" when the following hold [*Rodger et al.*, 2010]: e1 > 2 × P2, e2 > 2 × P3 and e3 > 2 × P3.

[14] On the other hand, a sharp enhancement of the precipitating electron flux at energies >30 keV is seen at 14:53:27 UT, indicating a "good" quality electron counts under the above criterion. The phenomenon was simultaneously observed at energies >100 keV and >300 keV, but at these energies it was less pronounced. As denoted by the green vertical solid line in Figure 2, the peak of precipitating electron flux was located at 67.20° geographical latitude (63.39° geomagnetic latitude). It has been found that the precipitation of energetic protons is latitudinally separated from that of energetic electrons. As shown in Figure 2, the peak of precipitating electron flux is equatorward to that of precipitating proton flux.

[15] Figure 3 shows the power spectrum density of the geomagnetic pulsation measured by the KIL, IVA and SOD stations. Between 14:42 UT and 15:00 UT, the increase of the pulsation intensity with frequencies of 0.2–0.4 Hz i.e., the band of Pc1, was detected by the three stations. Between 14:48 UT and 14:50 UT, the maximal intensity of Pc1 waves was observed at the IVA among those three stations.

Table 1. List of the Universal Time (UT), Magnetic Local Time (MLT), Geomagnetic Latitude (Mlat) and *L*-Value (*L*) for the Peak Flux for Precipitating Protons and Electrons Observed by the NOAA 15 and NOAA 16, as Well as for the Peak Amplitude for EMIC and ELF Hiss Waves Observed by the Cluster C1

	UT	MLT	Mlat	*L*
Fluxpmax NOAA16	14:50:00	14:06	73.56	8.59
Fluxemax NOAA16	14:49:46	14:07	72.78	7.92
AMEMICmax SC1	14:51:42	15:46	70.85	7.61
AMhissmax SC1	14:53:48	15:47	70.63	7.50
Fluxpmax NOAA15	14:53:45	17:11	64.43	5.59
Fluxemax NOAA15	14:53:27	17:12	63.39	5.21

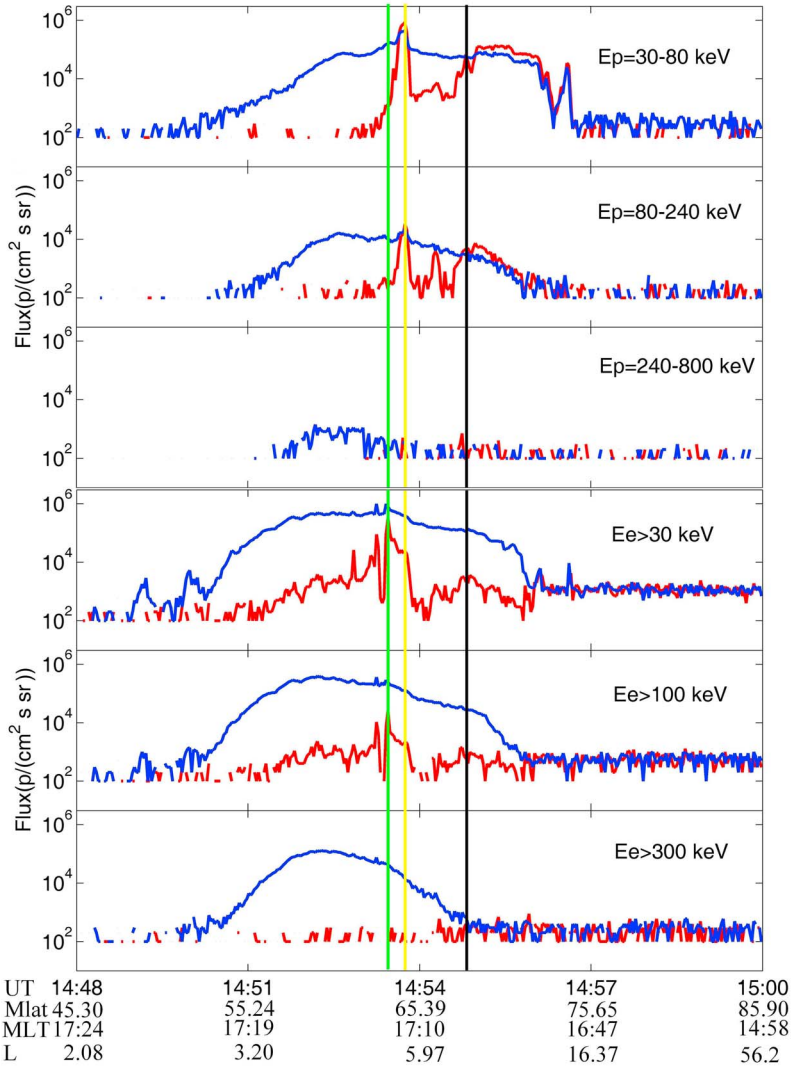

Figure 2. Particle data from the NOAA 15 on 18 July 2005. From the top is shown 30–80 keV protons, 80–240 keV protons, 240–800 keV protons, >30 keV electrons, >100 keV electrons and >300 keV electrons from both the 0° (red line) and 90° (blue line) MEPED detectors. The green and yellow vertical solid lines denote the location of peak flux for precipitating electrons and protons respectively. The black vertical solid line denotes the location of poleward boundary of anisotropic proton zone.

Thereafter, Pc1 wave intensity measured by the IVA was comparable to that of the SOD but larger than that of the KIL, implying that the source of such Pc1 waves firstly was located near the IVA and then moved toward the SOD. Since such a Pc1 wave is considered as a signature of an EMIC wave propagating off the equatorial plane to low altitudes [*Young et al.*, 1981; *Sakaguchi et al.*, 2008; *Morley et al.*, 2009], a sharp enhancement of the precipitating ion flux observed by NOAA15 at 14:53:45 UT is a result of RC ions scattered into the loss cone by EMIC waves.

[16] In Figure 4, blue and red lines show the trapped and precipitating flux intensities observed by the MEPED instrument of the NOAA 16, respectively. The black vertical solid line denotes the poleward boundary of the proton anisotropic zone, which is also the equatorial boundary of the proton isotropic zone at higher (auroral) latitudes. Within the anisotropic zone, a sharp enhancement of the precipitating ion flux, together with the prominent variation of the trapped flux intensity, is seen at 14:50:00 UT. As denoted by the yellow vertical solid line in Figure 4, the peak of precipitating proton flux was located at 68.57° geographical latitude (73.56° geomagnetic latitude). In this case, we can see that the precipitating flux in the first channel (Figure 4, first panel) is almost as intense as the mirroring flux, which serves as an indication of strong pitch angle scattering for ions with energies between 30 keV and 80 keV, while for the higher energies pitch angle diffusion is weaker. On the other hand, a sharp enhancement of the precipitating electron flux at energies >30 keV is seen at 14:49:46 UT, indicating a "good" quality electron counts under the above criterion. The phenomenon was simultaneously observed at energies >100 keV and >300 keV, but at these energies it was less

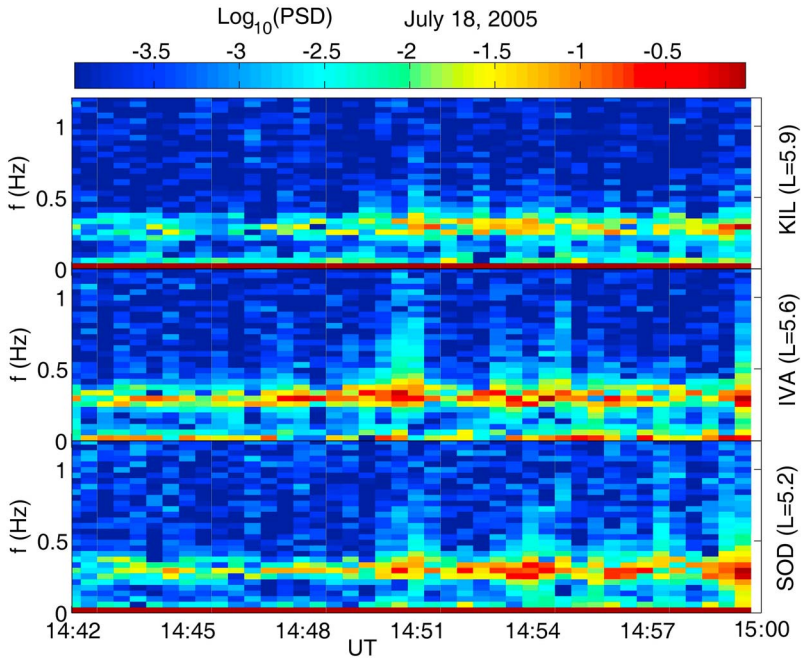

Figure 3. Power spectrum density of the D component (geomagnetic east–west) of geomagnetic pulsation measured by the KIL, IVA and SOD stations.

pronounced. As denoted by the green vertical solid line in Figure 4, the peak of precipitating electron flux was located at 67.87° geographical latitude (72.78° geomagnetic latitude). It has been found that the precipitation of energetic protons is latitudinally separated from that of energetic electrons. As shown in Figure 4, the peak of precipitating electron flux is equatorward to that of precipitating proton flux.

4. Discussion and Conclusion

[17] As mentioned above, the conjugate observations of the NOAA15 satellite and the Finnish network of search coil magnetometers have demonstrated that a sharp enhancement of the precipitating ion flux is a result of ring current ions scattered into the loss cone by EMIC waves. Within the anisotropic zone, a sharp enhancement of the precipitating ion flux leads to a detached proton arc [*Spasojević et al.*, 2004; *Yahnin et al.*, 2009; *Yuan et al.*, 2010]. The first global images of the Earth's proton aurora have been provided by the Far Ultraviolet (FUV) Spectrographic Imager (SI) [*Mende et al.*, 2000] onboard the IMAGE satellite [*Burch*, 2000]. On a number of occasions, arcs of precipitating protons have been observed at latitudes equatorward of and separated from the main proton oval [*Immel et al.*, 2002; *Burch et al.*, 2002]. As listed in Table 1, observations of the peak flux for precipitating protons and electrons by the NOAA 15 and NOAA 16, as well as the peak amplitude for EMIC and ELF hiss waves by the Cluster C1, focus on the interval of 14:49 UT–14:55 UT. In order to show the detached proton aurora during the interval, we check the data of the FUV SI12 instrument onboard the IMAGE spacecraft. Figure 5 shows two proton aurora images from FUV SI12 instrument onboard the IMAGE spacecraft at 14:49:27 UT and 14:55:42 UT on 18 July 2005. The pointing calculation depends on valid data from the star tracker. During the so-called "summer vacation" when the star tracker was not working, only interpolated spin axis data are used that are at times still inaccurate. Unfortunately, the "summer vacation" covers the time interval of interest in the paper. Therefore, we cannot obtain the mapping of proton aurora images into the southern/northern hemisphere. However, as shown in Figure 5 (top), a well-structured main proton oval with most strong intensity of proton aurora near the midnight can be easily recognized, which is caused by precipitating energetic protons from the magnetospheric plasma sheet within the isotropic region in Figure 2 or Figure 4. To be noted, a detached subauroral proton arc denoted by red fan-shaped lines can also easily be seen in Figure 5 (top), which should be in the afternoon or morning sector. The detached subauroral proton arc denoted by red fan-shaped lines kept well-structured between 14:49:27 UT and 14:55:42 UT. As shown in Figures 2 and 4, the NOAA 15 and NOAA 16 observed the peak flux for precipitating protons within the anisotropic zone at 17:11 MLT and 14:06 MLT in the afternoon sector, respectively. On the other hand, during the interval the NOAA 17 and NOAA 18 satellites did not observe obvious precipitating protons within the anisotropic zone in the morning sector (not shown here). Although we cannot project the footprint of the NOAA 15 or NOAA 16 satellite on the proton aurora image, it is reasonable that the subauroral proton arc is caused by the precipitating energetic ring current protons observed by the NOAA 15 or NOAA 16 satellite in the afternoon sector.

[18] On the other hand, between 14:48 UT and 14:55 UT in the region where the EMIC waves were observed by Cluster C1 in the plasmaspheric plume, Figure 4 of paper 1 has shown that the pitch angle distribution of ions became more isotropic due to the pitch angle scattering by the EMIC

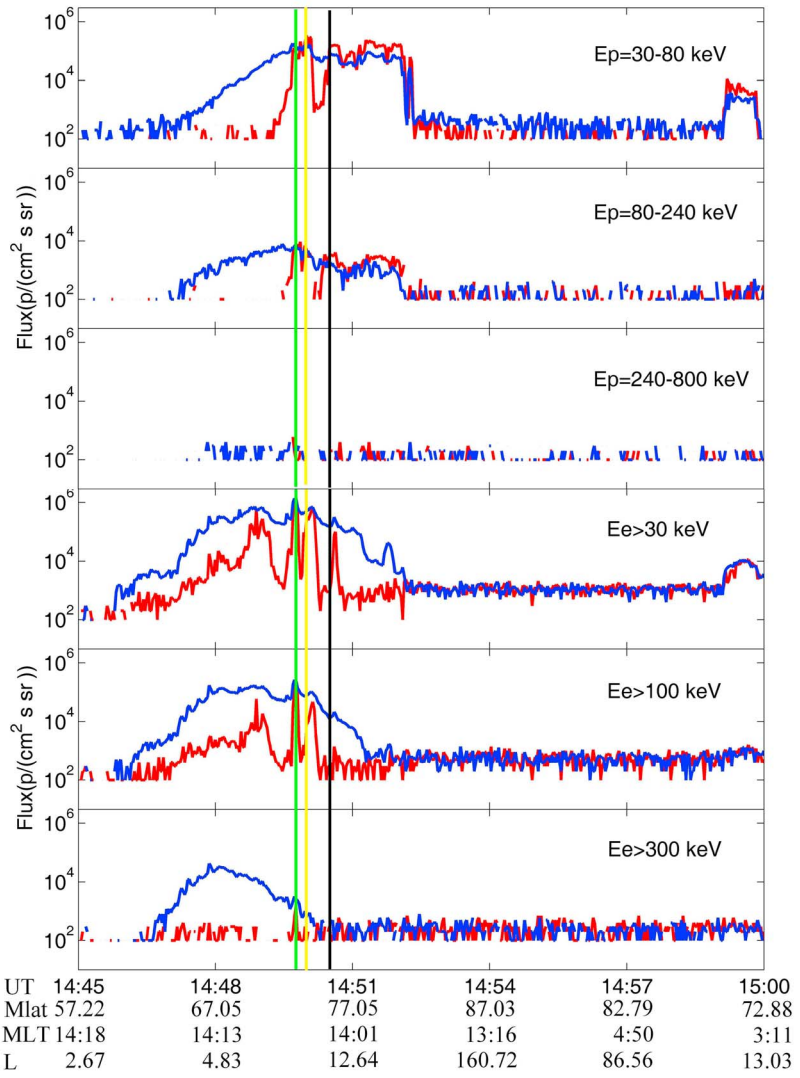

Figure 4. Particle data from the NOAA 16 on 18 July 2005. From the top is shown 30–80 keV protons, 80–240 keV protons, 240–800 keV protons, >30 keV electrons, >100 keV electrons and >300 keV electrons from both the 0° (red line) and 90° (blue line) MEPED detectors. The green and yellow vertical solid lines denote the location of peak flux for precipitating electrons and protons respectively. The black vertical solid line denotes the location of poleward boundary of anisotropic proton zone.

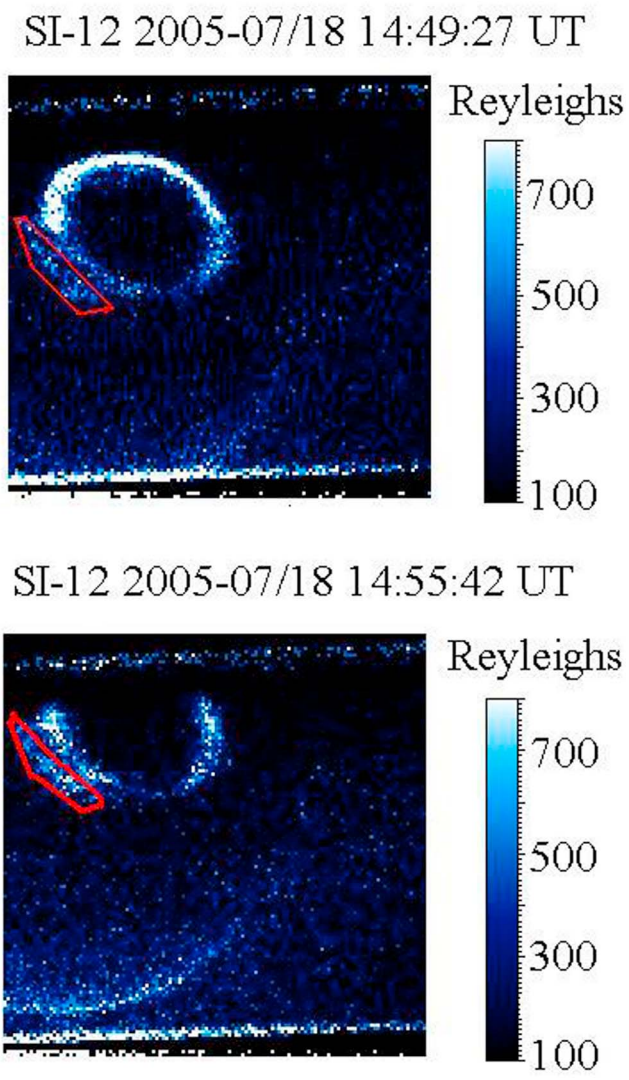

Figure 5. Proton aurora images from FUV SI12 instrument onboard the IMAGE spacecraft at 14:49:27 UT and 14:55:42 UT on 18 July 2005. Red fan-shaped line denotes a detached subauroral proton arc.

waves, which was discussed in detail in paper 1. As a result, RC ions scattered into the loss cone can cause subauroral arcs. As listed in Table 1, the Cluster C1 observed the peak amplitude for EMIC waves at 14:51:42 (15:46 MLT in the afternoon sector). Therefore, it is reasonable that the subauroral proton arc in Figure 5 is also caused by RC ions scattered into the loss cone in the plasmaspheric plume observed by Cluster C1. As shown in Figures 2 and 4, between 14:48 UT and 14:55 UT the NOAA 15 and the NOAA 16 observed precipitating energetic ions/electrons within the anisotropic zone at about 17:10–17:15 MLT and 14:05–14:15 MLT, respectively. As shown in Figure 4 of paper 1, during the same interval Cluster C1 simultaneously observed the EMIC waves and ELF hiss at about 15:40–15:50 MLT, between the location of precipitating energetic ions observed by the NOAA 15 and that of the NOAA16. Since the EMIC waves are detected in the outer boundary of the plasmaspheric plume [*Yuan et al.*, 2010, 2012], we may trace the location of the outer boundary of the plasmaspheric plume with RC ions scattered into the loss cone. As listed in Table 1, the Cluster C1 observed the peak amplitude for EMIC waves at 15:46 MLT (L = 7.61). The NOAA 15 and NOAA 16 observed the peak flux for precipitating protons within the anisotropic zone at 17:11 MLT (L = 5.59) and 14:06 MLT (L = 8.59) in the afternoon sector, respectively. The result is in agreement with the structure of the plasmaspheric plume from pre-midnight through post-noon local times, i.e., the outer boundary at earlier MLT is located at larger L-value [*Goldstein and Sandel*, 2005]. As listed in Table 1, at the same MLT with observations of NOAA15 or NOAA16 the peak of precipitating proton flux was located at higher L-value than that of precipitating electron flux, which is in agreement with the region separation of ELF hiss and EMIC waves observed by Cluster C1, i.e., the location of peak amplitude for EMIC waves was located at higher L-value than that for ELF hiss waves. Since the footprints of Cluster C1 and the NOAA15 or NOAA 16 were in the afternoon sector with separation of about 1:30 in MLT and EMIC-wave particle interactions are sometimes localized [*Nomura et al.*, 2012], the observation of Cluster C1 and the NOAA15 or NOAA 16 is not a good point-to-point conjugate experiment. For the plasmaspheric plume mentioned in this paper, *Darrouzet et al.* [2008] have demonstrated the plasmaspheric plume extending from pre-midnight through post-noon local times by plotting electron densities along the trajectories of four Cluster spacecrafts projected along the magnetic fields lines onto the GSM frame. As denoted by red fan-shaped lines in Figure 5, an obvious detached subauroral proton arc denoted by red fan-shaped lines kept well-structured between 14:49:27 UT and 14:55:42 UT. It is important that it is not a midday subauroral patch, subauroral proton flash or 1500 MLT auroral hot spot but a detached subauroral proton arc [*Frey*, 2007]. The detached subauroral proton arc is considered as a consequence of the EMIC waves-RC interaction in the plasmaspheric plumes [*Immel et al.*, 2002; *Burch et al.*, 2002; *Spasojević et al.*, 2004; *Yuan et al.*, 2010]. Therefore, it is reasonable to conclude that those wave activities (ELF hiss, EMIC waves) in plasmaspheric plumes observed by Cluster C1 and energetic ion/electron precipitation observed by the NOAA15 and NOAA 16 at ionospheric altitudes should be associated with the same plasmaspheric plume from pre-midnight through post-noon local times.

[19] In summary, conjugate observations of the NOAA 15 satellite and the Finnish network of search coil magnetometers have demonstrated that a sharp enhancement of the precipitating ion flux is a result of RC ions scattered into the loss cone by EMIC waves. Those precipitating RC ions lead to a detached subauroral proton arc. In addition, with observations of NOAA 15 and NOAA 16, the peak of precipitating electron flux was equatorward to that of precipitating proton flux, which is in agreement with the region separation of ELF hiss and EMIC waves observed by Cluster C1 shown in paper 1. In combination with the result of the paper 1, we demonstrate the link between the wave activities (ELF hiss, EMIC waves) in plasmaspheric plumes and energetic ion/electron precipitation at ionospheric altitudes. Therefore, it is an important characteristic of the plasmaspheric plumes-RC-ionosphere interaction during a geomagnetic storm that

the precipitation of energetic protons is latitudinally separated from that of energetic electrons.

[20] **Acknowledgments.** Data from the Finnish pulsation magnetometer chain were kindly provided by the Sodankylä Geophysical Observatory. NOAA MEPED data were provided by NOAA. Harald U. Frey kindly provided the proton aurora image from IMAGE FUV SI12. This research is supported by the National Natural Science Foundation of China (40974088, 41174140), research Fund for the Doctoral Program of Higher Education of China (20110141110043), and open Research Fund Program of the State Key Laboratory of Space Weather, Chinese Academy of Sciences. The work of A. G. Yahnin is supported by the Russian Academy of Sciences through the basic research program 22.

[21] Robert Lysak thanks the reviewers for their assistance in evaluating this paper.

References

Anderson, B. J., R. E. Erlandson, and L. J. Zanetti (1992), A statistical study of Pc1–2 magnetic pulsations in the equatorial magnetosphere: 1. Equatorial occurrence distributions, *J. Geophys. Res.*, *97*(A3), 3075–3088, doi:10.1029/91JA02706.

Bortnik, J., R. M. Thorne, and N. P. Meredith (2008), The unexpected origin of plasmaspheric hiss from discrete chorus emissions, *Nature*, *452*(6), 62–66, doi:10.1038/nature06741.

Burch, J. L. (2000), IMAGE mission overview, *Space Sci. Rev.*, *91*, 1–14, doi:10.1023/A:1005245323115.

Burch, J. L., et al. (2002), Interplanetary magnetic field control of afternoon-sector detached proton auroral arcs, *J. Geophys. Res.*, *107*(A9), 1251, doi:10.1029/2001JA007554.

Chan, K. W., and R. E. Holzer (1976), ELF hiss associated with plasma density enhancements in the outer magnetosphere, *J. Geophys. Res.*, *81*(13), 2267–2274, doi:10.1029/JA081i013p02267.

Chen, L., R. M. Thorne, V. K. Jordanova, C.-P. Wang, M. Gkioulidou, L. Lyons, and R. B. Horne (2010), Global simulation of EMIC wave excitation during the 21 April 2001 storm from coupled RCM-RAM-HOTRAY modeling, *J. Geophys. Res.*, *115*, A07209, doi:10.1029/2009JA015075.

Cornilleau-Wehrlin, N., R. Gendrin, F. Lefeuvre, M. Parrot, R. Grard, D. Jones, A. Bahnsen, E. Ungstrup, and W. Gibbons (1978), VLF electromagnetic waves observed onboard GEOS-1, *Space Sci. Rev.*, *22*, 371–382, doi:10.1007/BF00210874.

Cornilleau-Wehrlin, N., J. Solomon, A. Korth, and G. Kremser (1993), Generation mechanism of plasmaspheric ELF/VLF hiss: A statistical study from GEOS 1 data, *J. Geophys. Res.*, *98*(A12), 21,471–21,479, doi:10.1029/93JA01919.

Cornwall, J. (1965), Cyclotron instabilities and electromagnetic emission in the ultra low frequency and very low frequency ranges, *J. Geophys. Res.*, *70*(1), 61–69, doi:10.1029/JZ070i001p00061.

Darrouzet, F., J. De Keyser, P. M. E. Décréau, F. El Lemdani-Mazouz, and X. Vallières (2008), Statistical analysis of plasmaspheric plumes with Cluster/WHISPER observations, *Ann. Geophys.*, *26*, 2403–2417, doi:10.5194/angeo-26-2403-2008.

Darrouzet, F., et al. (2009), Plasmaspheric density structures and dynamics: Properties observed by the CLUSTER and IMAGE missions, *Space Sci. Rev.*, *145*(1–2), 55–106, doi:10.1007/s11214-008-9438-9.

Elphic, R. C., M. F. Thomsen, and J. E. Borovsky (1997), The fate of the outer plasmasphere, *Geophys. Res. Lett.*, *24*(4), 365–368, doi:10.1029/97GL00141.

Erlandson, R. E., and A. Ukhorskiy (2001), Observations of electromagnetic ion cyclotron waves during geomagnetic storms: Wave occurrence and pitch angle scattering, *J. Geophys. Res.*, *106*(A3), 3883–3895, doi:10.1029/2000JA000083.

Evans, D. S., and M. S. Greer (2004), Polar Orbiting Environmental Satellite Space Environment Monitor—2: Instrument descriptions and archive data documentation, *NOAA Tech. Memo. 1.4*, Space Environ. Lab., Boulder, Colo.

Fraser, B. J., and T. S. Nguyen (2001), Is the plasmaspause a preferred source region of electromagnetic ion cyclotron waves in the magnetosphere?, *J. Atmos. Terr. Phys.*, *63*, 1225–1247, doi:10.1016/S1364-6826(00)00225-X.

Frey, H. U. (2007), Localized aurora beyond the auroral oval, *Rev. Geophys.*, *45*, RG1003, doi:10.1029/2005RG000174.

Gamayunov, K. V., and G. V. Khazanov (2008), Crucial role of ring current H+ in electromagnetic ion cyclotron wave dispersion relation: Results from global simulations, *J. Geophys. Res.*, *113*, A11220, doi:10.1029/2008JA013494.

Gary, S. P., M. F. Thomsen, L. Yin, and D. Winske (1995), Electromagnetic proton cyclotron instability: Interactions with magnetospheric protons, *J. Geophys. Res.*, *100*(A11), 21,961–21,972, doi:10.1029/95JA01403.

Goldstein, J., and B. R. Sandel (2005), The global pattern of evolution of plasmaspheric drainage plumes, in *Inner Magnetosphere Interactions: New Perspectives From Imaging*, vol. 159, edited by J. L. Burch, M. Schulz, and H. Spence, pp. 1–22, AGU, Washington, D. C., doi:10.1029/159GM02.

Horne, R. B., and R. M. Thorne (1993), On the preferred source location for the convective amplification of ion cyclotron waves, *J. Geophys. Res.*, *98*(A6), 9233–9247, doi:10.1029/92JA02972.

Immel, T. J., S. B. Mende, H. U. Frey, L. M. Peticolas, C. W. Carlson, J.-C. Gérard, B. Hubert, S. A. Fuselier, and J. L. Burch (2002), Precipitation of auroral protons in detached arc, *Geophys. Res. Lett.*, *29*(11), 1519, doi:10.1029/2001GL013847.

Jordanova, V. K., M. Spasojević, and M. F. Thomsen (2007), Modeling the electromagnetic ion cyclotron wave-induced information of detached subauroral proton arcs, *J. Geophys. Res.*, *112*, A08209, doi:10.1029/2006JA012215.

Mende, S. B., et al. (2000), Far ultraviolet imaging from the IMAGE spacecraft. 3. Spectral imaging of Lyman-a and OI 135.6 nm, *Space Sci. Rev.*, *91*, 287–318, doi:10.1023/A:1005292301251.

Morley, S. K., S. T. Ables, M. D. Sciffer, and B. J. Fraser (2009), Multipoint observations of Pc1–2 waves in the afternoon sector, *J. Geophys. Res.*, *114*, A09205, doi:10.1029/2009JA014162.

Nomura, R., K. Shiokawa, K. Sakaguchi, Y. Otsuka, and M. Connors (2012), Polarization of Pc1/EMIC waves and related proton auroras observed at subauroral latitudes, *J. Geophys. Res.*, *117*, A02318, doi:10.1029/2011JA017241.

Parrot, M., and F. Lefeuvre (1986), Statistical study of the propagation characteristics of ELF hiss observed on GEOS 1, inside and outside the plasmasphere, *Ann. Geophys.*, *4*, 363–384.

Pasmanik, D. L., V. Y. Trakhtengerts, A. G. Demekhov, A. A. Lubchich, E. E. Titova, T. A. Yahnina, M. J. Rycroft, J. Manninen, and T. Turunen (1998), A quantitative model for cyclotron wave-particle interaction at the plasmapause, *Ann. Geophys.*, *16*, 322–330, doi:10.1007/s00585-998-0322-4.

Raben, V. J., D. S. Evans, H. H. Sauer, S. R. Sahm, and M. Huynh (1995), TIROS/NOAA Satellite Space Environment Monitor data archive documentation: 1995 update, *Tech. Memo. ERL SEL-86*, NOAA, Silver Spring, Md.

Rodger, C. J., M. A. Clilverd, J. C. Green, and M. M. Lam (2010), Use of POES SEM-2 observations to examine radiation belt dynamics and energetic electron precipitation into the atmosphere, *J. Geophys. Res.*, *115*, A04202, doi:10.1029/2008JA014023.

Russell, C. T., R. E. Holzer, and E. J. Smith (1969), OGO 3 observations of ELF noise in the magnetosphere: 1. Spatial extent and frequency of occurrence, *J. Geophys. Res.*, *74*(3), 755–777, doi:10.1029/JA074i003p00755.

Sakaguchi, K., K. Shiokawa, Y. Miyoshi, Y. Otsuka, T. Ogawa, K. Asamura, and M. Connors (2008), Simultaneous appearance of isolated auroral arcs and Pc1 geomagnetic pulsations at subauroral latitudes, *J. Geophys. Res.*, *113*, A05201, doi:10.1029/2007JA012888.

Sandanger, M., F. Søraas, K. Aarsnes, K. Oksavik, and D. S. Evans (2007), Loss of relativistic electrons: Evidence for pitch angle scattering by electromagnetic ion cyclotron waves excited by unstable ring current protons, *J. Geophys. Res.*, *112*, A12213, doi:10.1029/2006JA012138.

Sergeev, V. A., E. M. Sazhina, N. A. Tsyganenko, J. A. Lundblad, and F. Soraas (1983), Pitch-angle scattering of energetic protons in the magnetotail current sheet as the dominant source of their isotropic precipitation into the nightside ionosphere, *Planet. Space Sci.*, *31*, 1147–1155, doi:10.1016/0032-0633(83)90103-4.

Spasojević, M., and S. A. Fuselier (2009), Temporal evolution of proton precipitation associated with the plasmaspheric plume, *J. Geophys. Res.*, *114*, A12201, doi:10.1029/2009JA014530.

Spasojević, M., H. U. Frey, M. F. Thomsen, S. A. Fuselier, S. P. Gary, B. R. Sandel, and U. S. Inan (2004), The link between a detached subauroral proton arc and a plasmaspheric plume, *Geophys. Res. Lett.*, *31*, L04803, doi:10.1029/2003GL018389.

Summers, D., B. Ni, N. P. Meredith, R. B. Horne, R. M. Thorne, M. B. Moldwin, and R. R. Anderson (2008), Electron scattering by whistler-mode ELF hiss in plasmaspheric plumes, *J. Geophys. Res.*, *113*, A04219, doi:10.1029/2007JA012678.

Thorne, R. M., E. J. Smith, R. K. Burton, and R. E. Holzer (1973), Plasmaspheric hiss, *J. Geophys. Res.*, *78*(10), 1581–1596, doi:10.1029/JA078i010p01581.

Titova, E. E., et al. (1998), Strong localized variations of the low-altitude energetic electron fluxes in the evening sector near the plasmapause, *Ann. Geophys.*, *16*, 25–33, doi:10.1007/s00585-997-0025-2.

Yahnin, A. G., and T. A. Yahnina (2007), Energetic proton precipitation related to ion-cyclotron waves, *J. Atmos. Terr. Phys.*, *69*, 1690–1706, doi:10.1016/j.jastp.2007.02.010.

Yahnin, A. G., T. A. Yahnina, and A. G. Demekhov (2006), Interrelation between localized energetic particle precipitation and cold plasma inhomogeneities in the magnetosphere, *Geomagn. Aeron.*, Engl. Transl., *46*(3), 332–338, doi:10.1134/S0016793206030078.

Yahnin, A. G., T. A. Yahnina, H. U. Frey, T. Bösinger, and J. Manninen (2009), Proton aurora related to intervals of pulsations of diminishing periods, *J. Geophys. Res.*, *114*, A12215, doi:10.1029/2009JA014670.

Young, D. T., et al. (1981), Wave-particle interactions near observed on GEOS 1 and 2: 1. Propagation of ion cyclotron waves in He+ rich plasma, *J. Geophys. Res.*, *86*(A8), 6755–6772, doi:10.1029/JA086iA08p06755.

Yuan, Z., X. Deng, X. Lin, Y. Pang, M. Zhou, P. M. E. Décréau, J. G. Trotignon, E. Lucek, H. U. Frey, and J. Wang (2010), Link between EMIC waves in a plasmaspheric plume and a detached sub-auroral proton arc with observations of Cluster and IMAGE satellites, *Geophys. Res. Lett.*, *37*, L07108, doi:10.1029/2010GL042711.

Yuan, Z., L. Zhao, Y. Xiong, X. Deng, and J. Wang (2011), Energetic particle precipitation and the influence on the sub-ionosphere in the SED plume during a super geomagnetic storm, *J. Geophys. Res.*, *116*, A09317, doi:10.1029/2011JA016821.

Yuan, Z., Y. Xiong, Y. Pang, M. Zhou, X. Deng, J. G. Trotignon, E. Lucek, and J. Wang (2012), Wave-particle interaction in a plasmaspheric plume observed by a Cluster satellite, *J. Geophys. Res.*, *117*, A03205, doi:10.1029/2011JA017152.